The Comparison of Martensitic Transformation Sequences Between Aged Ti-50.6 and Ti-51.0 at.% Ni Alloys by in-situ SEM Observations

B. Karbakhsh Ravari*

Department of Applied Science for Electronics and Materials, Interdisciplinary Graduate School of Engineering Sciences, Kyushu University, Kasuga, Fukuoka, Japan.
Received: 13 March 2017 – Accepted: 17 April 2017

Abstract

The comparison of martensitic transformation sequences between aged Ti-50.6 and Ti-51.0 at.%Ni alloys have been investigated by differential scanning calorimetry (DSC) and in-situ scanning electron microscopy (SEM). Ti-50.6 and 51.0 at.% Ni alloys were selected for evaluation of Ni concentrations. These alloys were heat-treated at 1223 K for 3.6 ks and then aged at 773 K for 3.6 ks. Although the Ti-50.6 and 51 at. % Ni alloys revealed the triple stage transformations during cooling, but the results of in-situ SEM observations showed that the sequence of these transformations was completely different from each other. Although, the distribution and size of Ti_3Ni_4 precipitates observed in various compositions were different from each other, but the heterogeneity in distribution and size of precipitates was a common feature of them. For both of the compositions, martensitic transformation sequences are quantitatively proved by comparing DSC measurements and SEM observations. The calculations show good agreement between DSC cooling curve and SEM observation results.

Keywords: Ti-Ni Alloy, Multistage Martensitic Transformation, Ni Concentration.

1. Introduction

Mechanocaloric effects refer to the thermal response (adiabatic temperature and isothermal entropy changes) of a solid when subjected to an external stress. When the solid is in the vicinity of a structural first-order transition, these quantities can reach large values for moderate stresses giving rise to the so-called giant caloric effects [1–4]. These large values are related to the release (or absorption) of the latent heat associated with the first-order transition. From an applied point of view, giant caloric materials are good candidates for the development of an efficient environmental friendly solid state refrigeration technology [5]. Prominent among the materials exhibiting giant mechanocaloric effects are shape memory alloys. On cooling, these alloys undergo a transition from a high-temperature (high symmetry) cubic structure towards a lower-temperature (lower symmetry) close-packed structure. This is the martensitic transition which is first-order and difusionless, with a lattice distortion which is mostly given by a shear. Such a shear distortion is significantly large and makes the martensitic transition strongly sensitive to application of external uniaxial stress, which gives rise to a series of unique thermomechanical properties exhibited by these alloys such as shape memory effect, pseudoelasticity and superelasticity [6].

Ti-Ni Shape memory alloys at the near-equiatomic composition are interesting functional materials and frequently used in industrial and medical applications [7,8]. According to the phase diagram of Ti-Ni alloys, since the Ni-rich border of the B2 phase has a positive slope, it is obvious that with an increment of the temperature, the amount of Ni-solubility increase. So, obtaining of supersaturated Ni in the Ti-Ni matrix by quenching is possible and subsequently precipitation reaction can occur upon aging at relatively low temperature. During precipitation, formation of Ni-rich precipitates cause to decrement of the Ni content in the Ti-Ni matrix. Consequently the transformation temperature tends to increase upon aging. In this way, size, density and distribution type of precipitates are very important factors which affect on the martensitic transformation, strongly. Because of these effects, multistage martensitic transformation (MMT) behavior has been observed for aged Ni-rich Ti-Ni alloys [9-22]. In near-equiatomic Ti-Ni alloys, the martensitic transformation can occur as either as single-stage transformation (B2 → M) or as double-stage transformation (B2 → R → M), depending on the heat treatment conditions [8]. Under certain aging conditions, more complex triple-[10-16, 19-21] and quadruple-stage transformation [22,23-25] have been observed by differential scanning calorimetry (DSC). In this study, we refer to the triple-stage transformations as B2 → R → M_1 → M_2. It is obvious that with changing Ni concentration, the amount of supersaturation of Ni in Ti-Ni matrix will change and subsequently different size, density and distribution type of precipitates will appear. In

*Corresponding author
Email address: banafsheh.karbakhsh.r@gmail.com

this way, we expect that different types of MMT occur. Several experimental studies were performed to evaluate the effect of Ni-concentration on martensitic transformation in Ti-Ni alloys [23-28]. But these effects on MMT are not cleared yet. The present study was performed in order to finding the sequences of martensitic transformation in two different Ni-concentration of Ti-Ni shape memory alloys by means of DSC measurements and in-situ SEM observations.

2. Materials and Methods

The commercially available Ti-50.6 and 51.0 at.% Ni alloys rods with 3 mm in diameter are used in the present study. The rods were cut into disks of about 1 and 0.5 mm in thickness for DSC measurements and SEM observations, respectively. In order to evaluate the martensitic transformation sequences of these specimens, disks were solution-treated at 1223 K for 3.6 ks and then quenched in ice water. In order to control the heat treatment atmosphere, the disks were sealed in an evacuated quartz tube of 2.5×10^{-4} pa as an unregulated atmosphere. Some other disks were solution treated and aged the same as the previous conditions under regulated atmosphere. These heat treatment atmosphere is controlled as illustrated in Fig. 1.

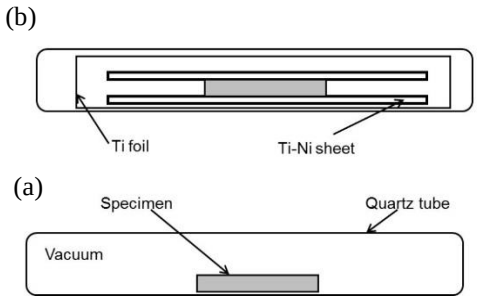

Fig. 1. Schematic illustrations of heat treatment conditions under (a) unregulated and (b) regulated atmosphere.

Some of the disks were sealed in an evacuated quartz tube of 2.5×10^{-4} Pa as shown in Fig. 1a . The rest disks were sandwiched between Ti-Ni sheets with the same chemical composition. Subsequently, they were wrapped with pure Ti foil of 0.02 mm (20 μm) in thickness and then sealed in an evacuated quartz tube of 2.5×10^{-4} Pa as shown in Fig. 1b . The disks heat treated by the former and latter conditions, are referred to the unregulated and regulated atmosphere, respectively.

After that, DSC measurements were performed by using a calorimeter (DSC-60, Shimadzu) with cooling and heating rate of 0.17 K/s. For SEM observations, the disks were electropolished in HNO_3/CH_3OH solution (1:3 in v/v). SEM observations were carried out in the Carl Zeiss-ULTRA55 equipped with angular selected back scattered electron (AsB) detector. A Peltier stage (Coolstage, Deben) with a working temperature of 320-220 K was used for in-situ SEM observations.

3. Results and Discussion

3.1. DSC Observations

Fig. 2. shows the DSC curves of Ti-50.6 and 51 at.% Ni alloys, which were aged at 773 K for 3.6 ks after solution treatment at 1223 K for 3.6 ks under unregulated atmosphere, respectively. Ti-50.6 and 51 at.% Ni alloys revealed the triple-stage transformations (B2→R→M1→M2) upon cooling. In this way, two martensitic peaks denoted as M1 and M2 were appeared in addition to R-peak during cooling. Three endothermic peaks denoted as A2, AR and A1 were observed for Ti-50.6 at. % Ni alloy during heating, meanwhile two endothermic peaks denoted as A2 and A1+AR were characterized from the DSC heating curve of Ti-51 at. % Ni alloy upon heating. From the thermal cycle experiments, the following relations between the endothermic and exothermic peaks were confirmed. For Ti-50.6 at.% Ni, the peaks A2, AR and A1 correspond to the peaks M2, R and M1, respectively. Fig. 1b shows that for Ti-51 at.% Ni alloy, reverse of first martensitic transformation and reverse of R-Phase transformation will be occurred simultaneously. It means that peak A2 corresponds to M2 and Peak A1+AR relates to peaks M1 and R. From the DSC results shown at Fig. 1., it can be concluded that changing of Ni-concentration for aged Ni-rich Ti-Ni alloys cause to change martensitic transformation behavior and consequently sequence of MMT, respectively.

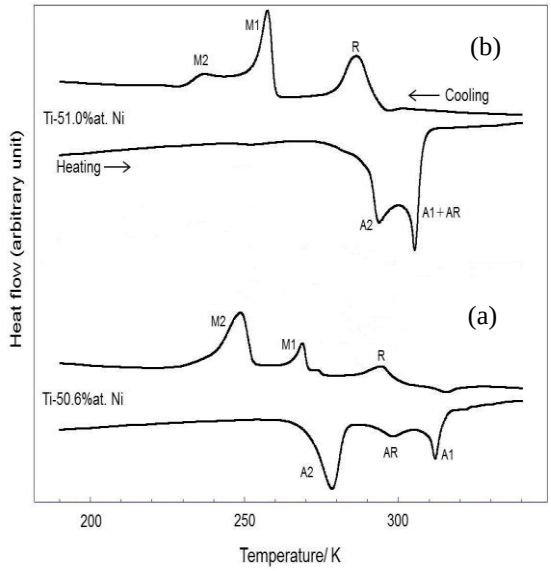

Fig. 2. DSC cooling and heating curves for Ti-50.6 and 51 at.% Ni alloys aged at 773 K for 3.6 ks after solution-treated at 1223 K for 3.6 ks under unregulated atmosphere.

Fig. 3. shows DSC curves for aged Ti-50.6and 51 at.% Ni alloys at 773 K for 3.6 ks after solution treatment at 1223 K for 3.6 ks under regulated atmosphere, respectively. All DSC cooling curves exhibit the double-stage transformation, B2→R→M, without any MMT behavior. It has been reconfirmed that the regulation of the heat treatment atmosphere prevents the MMT the same as previously published results [18, 19, 29, 30].

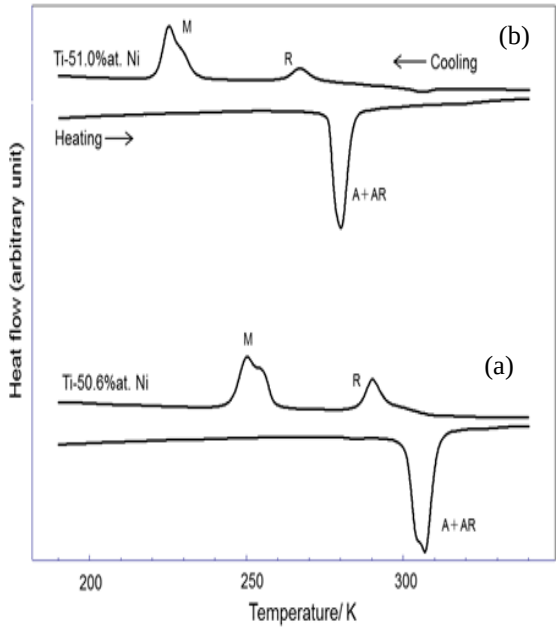

Fig. 3. The DSC cooling and heating curves for Ti-50.6 and 51 at.% Ni alloys aged at 773 K for 3.6 ks after solution treatment at 1223 K for 3.6 ks under regulated conditions.

3.2. Effect of Ni concentration on initial microstructure

In order to characterize the effect of Ni-concentration on MMT in aged Ni-rich Ti-Ni alloys, at first the initial microstructure observations were performed at room temperature. Fig. 4a shows a low magnification SEM-AsB image of the Ti-50.6 at.% Ni alloy aged at 773 K for 3.6 ks under unregulated atmosphere after electropolishing about 260 K. According to Fig. 1., this temperature was subjected between M1 and M2 peaks in the DSC cooling curve and SEM observation was performed at room temperature. From the DSC heating curve, it is obvious that at this temperature the reverse of first martensitic transformation doesn't occur. So, it was expected that martensitic phase corresponding to M1 peak should be visible in SEM observations. The M1 phase with brighter contrast was observed around the grain boundaries. Fig. 4b and c shows the enlarged micrographs taken from the areas B and C in Fig. 4a, respectively.

The heterogeneous distribution and size of Ti_3Ni_4 precipitates is obvious between grain interior and grain boundary. The apparent average diameter from grain interior to grain boundary was estimated to be between 650 and 350 nm. Fig. 5a shows a low magnification SEM-AsB image of the Ti-51 at.% Ni alloy aged at 773 K for 3.6 ks under unregulated atmosphere after electropolishing about 245 K. It was expected that the martensitic phase with bright contrast corresponding to the M1 peak should be observed in the specimen because of the electropolishing and observation conditions were the same as previous specimens.

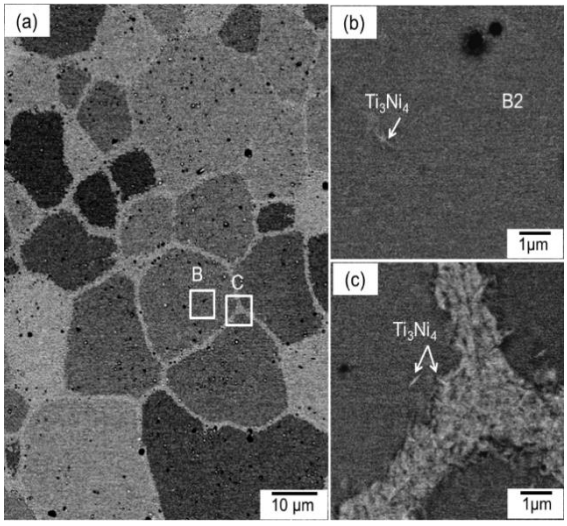

Fig. 4. (a) Low-magnification SEM-AsB image of the Ti-50.6 at.% Ni alloy aged at 773 K for 3.6 ks after solution treatment at 1223 K for 3.6 ks under unregulated atmosphere. (b), (c) Enlarged SEM-AsB images taken from areas B and C in (a), showing the grain interior and grain boundary, respectively.

The M1 phase with bright contrast was observed in the grain interior. Also, according to Fig. 5b and c which related to enlarged micrographs taken from area b and c, the heterogeneous distribution and size of precipitates are completely appeared from grain interior toward the grain boundary. In this way, it can be distinguished that from grain interior to grain boundary, the density of precipitates increases but the apparent average diameter decreases. The apparent average diameter of Ti_3Ni_4 precipitates from grain interior to grain boundary is estimated to be 270 and 75 nm. These different types of precipitates distribution can be explained by the difference between the degrees of Ni supersaturation by changing of Ni concentration in Ti-Ni alloy compositions. From these results it can be concluded that changing of Ni concentration cause to change the distribution and size of Ti_3Ni_4 precipitates in the specimens. This is consistent with previously published results [29, 30].

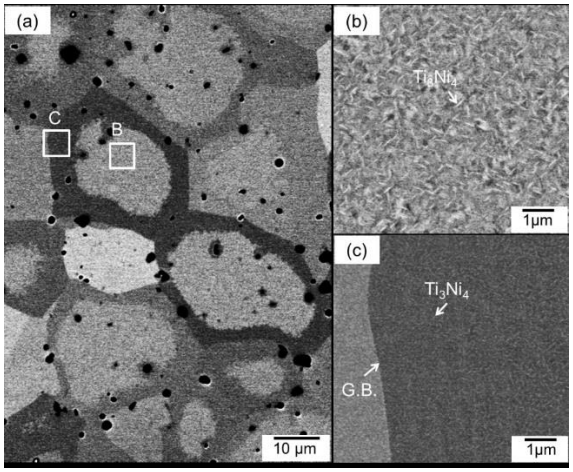

Fig. 5. (a) Low-magnification SEM-AsB image of the Ti-51 at.% Ni alloy aged at 773 K for 3.6 ks after solution treatment at 1223 K for 3.6 ks under unregulated atmosphere. (b), (c) Enlarged SEM-AsB images taken from areas B and C in (a), showing the grain interior and the grain boundary, respectively.

However, results of SEM observations for all of specimens aged under regulated atmosphere showed a homogeneous distribution and size of Ti_3Ni_4 precipitates for them. In order to see the microstructure and consequently the behavior of these alloys during martensitic transformation, the result of Ti-50.6 at.% Ni alloy aged at 773 K for 3.6 ks under regulated atmosphere is presented in this paper. For SEM observation, it electropolished about 270 K in the R-phase state. Because of the SEM observation were performed at room temperature, according to the DSC heating curve of this alloy, it is obvious that the reverse transformation didn't occur and it is expected that the microstructure should be completely martensite.

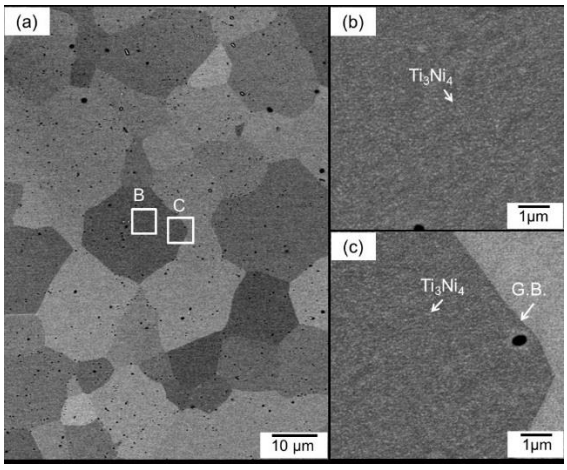

Fig . 6. (a) Low-magnification SEM-AsB images of the Ti-50.6 at.% Ni alloy aged at 773 K for 3.6 ks after solution treatment at 1223 K for 3.6 ks under regulated conditions. (b), (c) Enlarged SEM-AsB images taken from areas B and C in (a), showing grain interior and the grain boundary, respectively.

So, in order to see transformation behavior in this alloy, at first the specimen heated up to 323 K until the reverse transformation fully transformed to the parent phase and then cooled to the room temperature. Fig. 6a shows a low magnification SEM-AsB image of the aged Ti-50.6 at.% Ni alloy under regulated atmosphere. The enlarged micrographs in Fig. 6b and c show homogenous distribution and size of Ti_3Ni_4 precipitates at both the grain interior and grain boundary. The apparent average diameter at grain interior and grain boundary was about 60 nm. From these results it can be concluded that although changing of Ni concentration cause to change the distribution and size of Ti_3Ni_4 precipitates in the specimens, but by using of regulated atmosphere during heat treatment, no composition gradient created in the grains. On the other hand, for all of the specimen heat treated under unregulated atmosphere, there is a composition gradient between grain interior and grain boundary. This is consistent with previously published results [29, 30].

3.3. Effect of Ni concentration on multistage martensitic transformation

In order to evaluate the effect of Ni concentration on MMT, in-situ SEM observations were performed for all of specimens aged under unregulated atmosphere. Fig. 7. shows a series of in-situ SEM images of Ti-50.6 at.% Ni alloy aged at 773 K for 3.6 ks under controlled conditions during the cooling (a-d) and heating (e-h), respectively. The heterogeneous distribution and size of the Ti_3Ni_4 precipitates were observed between the grain interior and the grain boundary (Fig. 4.), although this was not visible in the low-magnification images (Fig. 7.). According to Fig. 7b, the first martensitic transformation corresponded to the M1 peak in the DSC cooling curve occurred around the grain boundary. With continuous cooling, the second martensitic transformation corresponded to the M2 peak, occurred in the grain interior (Fig. 7c and d). V-shaped, triangular, and hexangular surface reliefs, which are typical self-accommodation morphologies of B19' martensite, were clearly observed in grain interior [31]. According to Fig.7(e-g), upon heating at first the surface reliefs in the grain interior disappeared in the reverse order of their appearance. Finally, the B19' phase around the grain boundary completely disappeared (Fig. 7h). Fig. 8. shows a series of in-situ SEM images of Ti-51 at.% Ni alloy aged at 773 K for 3.6 ks under unregulated conditions during the cooling (a-d) and heating (e-h), respectively. The distribution and size of the Ti_3Ni_4 precipitates between the grain interior and the grain boundary were heterogeneous (Fig. 5.), meanwhile this was not clearly visible in the low-magnification images (Fig. 8.). Fig. 8b shows that the first martensitic transformation corresponded to the M1

peak in the DSC cooling curve occurred in the grain interior. Then, with continuing cooling, the martensitic formation developed toward the grain boundary (Fig. 8c) and finally completed around the grain boundary according to Fig. 8d.

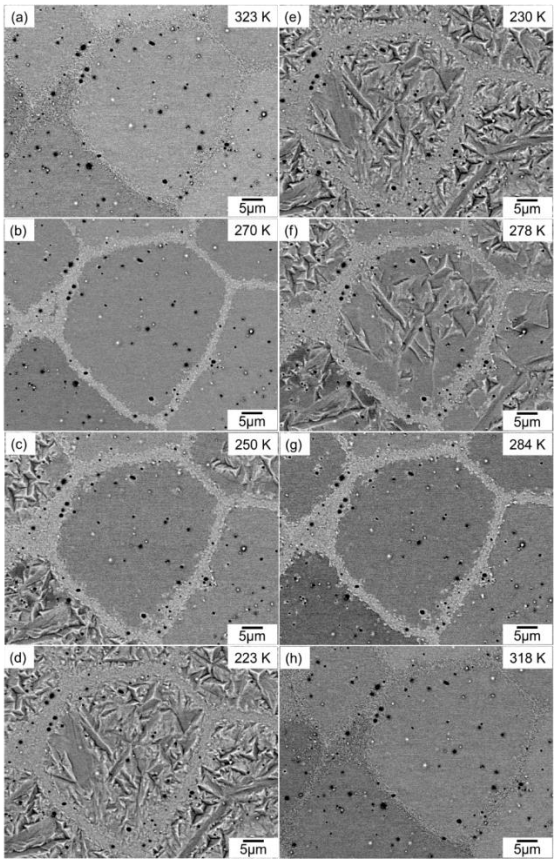

Fig. 7. A series of SEM-AsB images upon in-situ cooling and heating of the Ti-50.6 at.% Ni alloy aged at 773 K for 3.6 ks after solution treatment at 1223 K for 3.6 ks under unregulated conditions at (a) 323 K, (b) 270 K, (c) 250 K, (d) 223 K, (e) 230 K, (f) 278 K, (g) 284 K, and (h) 318 K.

So, the second martensitic transformation corresponded to the M2 peak, occurred in the grain boundary. Fig. 8 (e-g) show the sequence of reverse transformation for Ti-51 at. % Ni alloy upon heating. Grain boundary is the first area that reverse transformation occurs (Fig. 8f). Finally, the B19' phase at grain interior completely disappeared (Fig. 8h). By comparison of the obtained results from the in-situ SEM observations, the effect of Ni-concentration on MMT with considering constant aging conditions can be concluded. According to phase diagram of Ti-Ni alloys, with the changing of Ni-concentration the amount of Ni- supersaturation will change and subsequently the different types of Ti_3Ni_4 precipitates distribution can be obtained. So, various types of MMT will create accordingly.
Fig. 9. shows this effect schematically. The results can be summarized as follows:

A triple - stage transformation occurred at Ti-50.6 and 51 at. % Ni alloys, meanwhile for Ti-50.6 at. % Ni alloy, at the first area, near the grain boundary transforms to martensite and then grain interior is the second part of the grain which transforms to martensite. In contrast to it for Ti-51 at. % Ni alloy, firstly grain interior transforms to martensite and then martensitic transformation occurs in the area near the grain boundary.

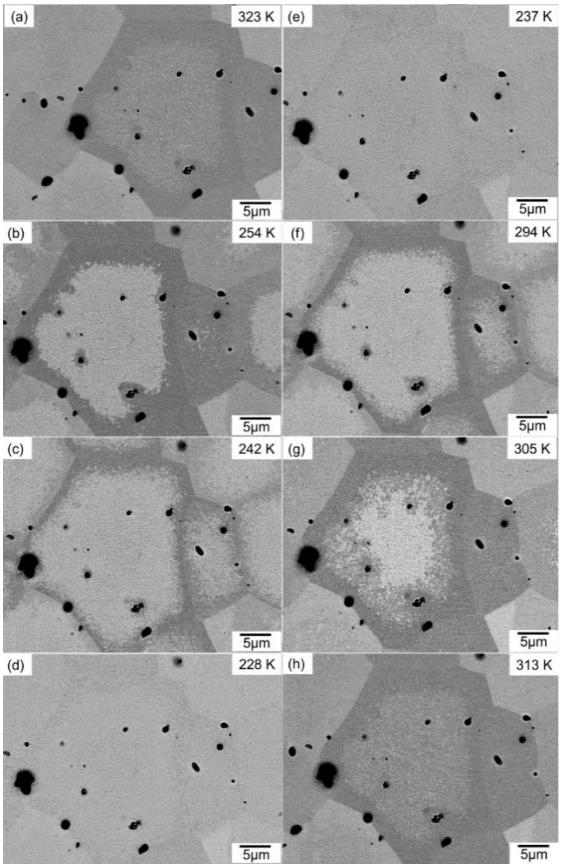

Fig. 8. A series of SEM-AsB images during in-situ cooling and heating of Ti-51.0 at.% Ni alloy aged at 773 K for 3.6 ks after solution treatment at 1223 K for 3.6 ks under unregulated conditions at (a) 323 K, (b) 254 K, (c) 242 K, (d) 228 K, (e) 237 K, (f) 294 K, (g) 305 K, and (h) 313 K.

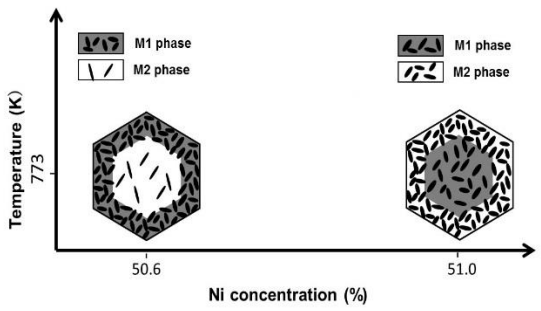

Fig. 9. Schematic illustration of the effect of Ni concentrations on the microstructures and sequences of the forward martensitic transformations in aged Ni-rich Ti-Ni alloys at 773 K for 3.6 ks.

In author's previous publications, quantitative analysis of transformation sequences for quadruple-stage transformation which occurs in Ti-50.8 at.% Ni alloy during cooling were performed based on comparison between the DSC peaks and the transformation area ratio in the EBSD [32] and SEM [30] images, respectively. Here, the quantitative analysis of transformation sequences for triple-stage transformations which occurs in Ti-50.6 and 51 at.% Ni alloys during cooling are investigated based on the comparison between the DSC peaks and the transformation area ratio in the SEM images. The following equations were applied in order to comparison of the mentioned areas for both of Ti-50.6 and 51 at. % Ni alloys as follows while the M_{1S} and M_{2S} are completely different depending on each composition:

$$M_{1D} / (M_{1D} + M_{2D}) = M_{1S} / (M_{1S} + M_{2S}) \quad (1)$$

$$M_{2D} / (M_{1D} + M_{2D}) = M_{2S} / (M_{1S} + M_{2S}) \quad (2)$$

where M_{1D} and M_{2D} are the M1 and M2 peak areas in the DSC cooling curves of Ti-50.6 and 51 at. % Ni alloys in Fig. 1. M_{1S} and M_{2S} correspond to the two different microstructure regions in the SEM images shown in Fig. 4. and Fig. 5. for Ti-50.6 and 51 at.% Ni alloys, respectively. SEM areas of M_{1S} and M_{2S} are the outer and center regions of the grain for Ti-50.6 at.% Ni alloy, while according to in-situ SEM observation for Ti-51 at.% Ni alloy, the center and outer regions of the grains are considered as M_{1S} and M_{2S}, respectively. The calculated values for the triple-stage transformations related to Ti-50.6 and 51 at.% Ni alloys are listed in Tables 1 and 2, respectively. The transformation events upon cooling were in good agreement. From these results, the correspondence between the exothermic peaks (M1 and M2) in the DSC cooling curves and transformation areas, and thus the sequence of forward martensitic transformations, was systematically established for these compositions.

Fig. 10. shows a series of in-situ SEM images of Ti-50.6 at.% Ni alloy aged at 773 K for 3.6 ks under regulated conditions during the cooling (a-d) and heating (e-h), respectively. The results show that martensitic transformation occurred randomly, irrespective of the grain boundary or the grain interior (Fig. 10(b-d)). The temperature range of the martensitic transformation was consistent with that of the M peak in the DSC cooling curve in Fig. 3. The bright contrast caused by the martensitic phase randomly disappeared upon heating (Fig. 10(e-h)). Same behavior for martensitic transformation were obtained for aged Ti-51 at.% Ni alloys under regulated atmosphere. By using of in-situ SEM results, sequences of forward and reverse martensitic transformation in different Ni-concentrations have been discussed. However, the R-phase transformation was not detected, because its transformation strain is small in comparison with that of the martensitic transformation. The R-phase transformation probably occurred in a restricted area in the specimens aged under controlled conditions, because the precipitate size and distribution of the Ti_3Ni_4 phase was heterogeneous. Although, the distribution and size of precipitates were homogeneous in the specimen aged under regulated atmosphere (Fig. 6.) and it can be concluded that the R-phase transformation occurred in the whole of the grain. The calculation for R-phase transformations are performed for Ti-50.6 and 51 at.% Ni alloys. It is obvious that the ratio of the R and M peaks in the DSC cooling curve should be constant when the transformations occur successively in the same area. According to this assumption same equation can be written for Ti-50.6 and 51 at.% Ni alloys aged at 773 K as follows:

$$R / M = R_D / M_{1D} \quad (3)$$

$$R \cdot M_{1S} / M (M_{1S} + M_{2S}) = R_D / (M_{1D} + M_{2D}) \quad (4)$$

where R and M are the R and M peak areas in the DSC cooling curve of the Ti-50.6 and 51 at.% Ni alloys aged under regulated conditions in Fig. 3., and R_D is the R peak area in the DSC cooling curves of the mentioned specimens aged under unregulated conditions in Fig. 2.

Table 1. Calculated values of equations (1) and (2), which shows that the exothermic peak ratio in the DSC cooling curve and the transformation area ratio in the SEM image for each of the martensitic transformations are comparable in Ti-50.6 at.% Ni aged at 773 K for 3.6 ks after solution treatment at 1223 K for 3.6 ks under unregulated conditions.

M1		M2	
$M_{1D} / (M_{1D} + M_{2D})$	$M_{1S} / (M_{1S} + M_{2S})$	$M_{2D} / (M_{1D} + M_{2D})$	$M_{2S} / (M_{1S} + M_{2S})$
0.30	0.27	0.70	0.73

Table 2. Calculated values of equations (1) and (2), indicating that the exothermic peak ratio in the DSC cooling curve and the transformation area ratio in the SEM image for each of martensitic transformations were comparable in Ti-51.0 at.% Ni aged at 773 K for 3.6 ks after solution treatment at 1223 K for 3.6 ks under unregulated conditions.

M1		M2	
$M_{1D}/(M_{1D}+M_{2D})$	$M_{1S}/(M_{1S}+M_{2S})$	$M_{2D}/(M_{1D}+M_{2D})$	$M_{2E}/(M_{1E}+M_{2E})$
0.77	0.74	0.23	0.26

The obtained results are listed in Tables 3 and 4. The results show that the R-Phase transformations for triple-stage transformations correspond to Ti-50.6 and 51 at.% Ni alloys were in good agreement. Therefore, It can be concluded that the R-phase transformation occurs only around the grain boundary in the Ti-50.6 at.% Ni alloy aged at 773 K, meanwhile grain interior is the area that R-phase transformation happens for aged Ti-51 at.% Ni alloy.

3.4. Effect of Ni concentration on reverse martensitic transformation

In the previous section, the forward multistage martensitic transformations for different compositions were specified. Also, the sequence of the reverse transformation for quadruple-stage transformation was explained elsewhere [30]. In the triple-stage transformation for Ti-50.6 at.% Ni alloy, during reverse transformation, at first the M2 phase in the center of the grain directly reverted to the B2 phase (Fig. 2a) and then reverse of R-Phase transformation and subsequently reverse of the M1 phase transformation around the grain boundary were occurred to B2 phase. For Ti-51 at.% Ni alloy, firstly the reverse transformation of the M2 phase occurs around the grain boundary and it directly transformed to the B2 phase (Fig. 2b) and then reverse of R-Phase transformation and M1 phase at center part of grains were occurred to B2 phase, simultaneously.

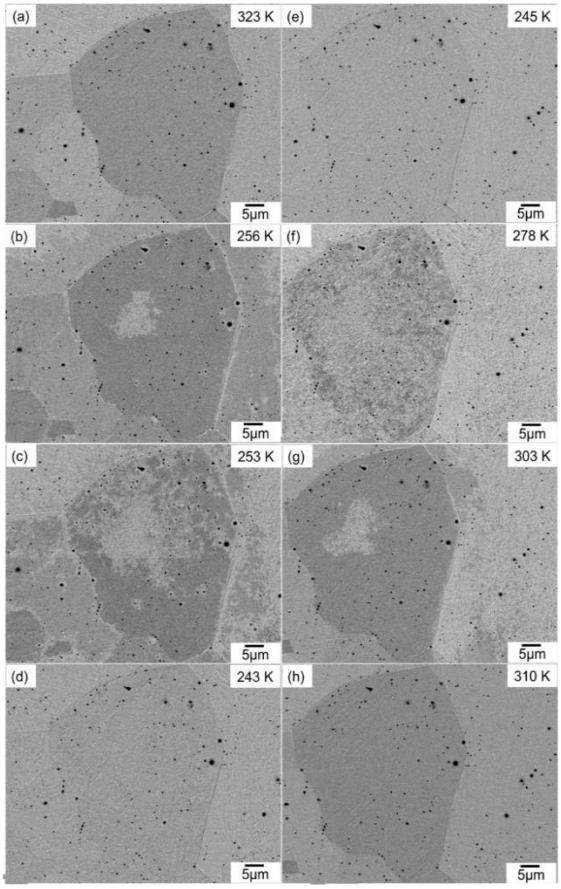

Fig. 10. A series of SEM-AsB images during in-situ cooling and heating of Ti-50.6 at.% Ni alloy aged at 773 K for 3.6 ks after solution treatment at 1223 K for 3.6 ks under regulated conditions at (a) 323 K, (b) 256 K, (c) 253 K, (d) 243 K, (e) 245 K, (f) 278 K, (g) 303 K, and (h) 310 K.

Table 3. Calculated values of equations (3) and (4) for the formation area of the R-phase in the triple-stage transformation in Ti-50.6 at.% Ni aged at 773 K for 3.6 ks after solution treatment at 1223 K for 3.6 ks under unregulated conditions.

R-phase			
R/M	R_D/M_{1D}	$R.M_{1S}/M(M_{1S}+M_{2S})$	$R_D/(M_{1D}+M_{2D})$
0.56	0.54	0.15	0.16

Table 4. Calculated values of equations (3) and (4) for the formation area of the R-phase in triple-stage transformation in Ti-51.0 at.% Ni aged at 773 K for 3.6 ks after solution treatment at 1223 K for 3.6 ks under unregulated conditions.

R-phase			
R/M	R_D/M_{1D}	$R.M_{1S}/M(M_{1S}+M_{2S})$	$R_D/(M_{1D}+M_{2D})$
0.92	0.93	0.69	0.71

4. Conclusions

The effect of Ni concentration on MMT in aged Ni-rich Ti-Ni alloys was evaluated by using of DSC measurements and in-situ SEM observations. The results are summarized as follows;

1. The Ti-50.6 and 51 at.% Ni alloys aged at 773 K for 3.6 ks under unregulated atmosphere show the different types of MMT.
2. The Ti-50.6 and 51 at.% Ni alloys exhibit the triple-stage transformation with the sequence of B2 → R → M1 → M2 while the areas related to M1 and M2 peaks for each composition were different from each other.
3. For Ti-50.6 at. % Ni alloy, the first martensitic transformation corresponding to M1 peak via the R-phase takes place at the grain boundary. Then, the transformation related to M2 peak occurs in the center part of the grain.
4. The transformed areas related to M1 peak via the R-phase and M2 peak for Ti-51 at. % Ni alloy were reverse of transformed areas which specified for Ti-50.6 at. % Ni alloy.
5. These transformation sequences are quantitatively proved by comparing the SEM images with DSC cooling curves.

References

[1] S.F.¨ahler, U.K. R¨ossler, O. Kastner, J. Eckert, G. Eggeler, H. Emmerich, P. Entel, S. M¨uller, E. Quandt and A. Karsten, Adv. Eng. Mater., 14(2012), 10.
[2] L. Ma˜nosa, A. Planes and M. Acet, J. Mater. Chem. A, 1(2013), 4925.
[3] X. Moya, S. Kar-Narayan and N.D. Mathur, Nature Mater. , 13 (2014), 439.
[4] X. Moya, E. Defay, V. Heine and N.D. Mathur, Nature Phys., 11 (2015), 202.
[5] A. Kitanovski, U. Plaznik, U. Tomc and A. Poredos, Int. J. Refrig., 57(2015), 288.
[6] K. Otsuka, T. Kakeshita, MRS Bull., 27(2002), 91.
[7] T. Saburi In: K. Otsuka, C.M. Wayman, editors. Shape memory materilas, Cambridge University Press, Cambridge, (1998), 49.
[8] J. Van Humpback, Mater. Sci. Eng. A, 273-275 (1999), 134.
[9] G. Fan, W. Chen, S. Yang, J. Zhu, X. Ren and K. Otsuka, Acta Mater., 52(2004), 4351.
[10] D. Favier, Y. Liu and P.G. Mc Cormick, Scripta Metall. Mater., 28(1993), 669.
[11] M.C. Carroll, Ch. Somsen and G. Eggeler, Scripta Mater., 50(2004), 187.
[12] A. Dlouhy, J. Khalil-Allafi and G. Eggeler, Philos. Mag., 83(2003), 339.
[13] P.C. Su, S.K. Wu, Acta Mater. , 52(2004), 1117.
[14] T. Tadaki, Y. Nakata, K. Shimizu and K. Otsuka, Trans. JIM, 27(1986), 731.
[15] L. Bataillard, J-E Bidaux and R. Gotthardt, philos. Mag. A, 78(1998), 327.
[16] J. Khalil-Allafi, X. Ren and G. Eggeler, Acta Mater. , 50(2002), 793.
[17] J. Khalil-Allafi, A. Dlouhy and G. Eggeler, Acta Mater. , 50(2002), 4255.
[18] M. Nishida, T. Hara, T. Ohba, K.Yamaguchi, K. Tanaka and K. Yamauchi, Mater. Trans., 44 (2003), 2631.
[19] K. Fujishima, M. Nishida, Y. Morizono, K. Yamaguchi, K. Ishiuchi and T. Yamamuro, Mater. Sci. Eng. A, 438-440(2006), 489.
[20] J. Khalil-Allafi, G. Eggeler, A. Dlouhy, W.W. Schmhal and C. Somsen, Mater. Sci. Eng. A, 378 (2004), 148.
[21] G. Fan, Y. Zhu, W. Chen, S. Yang, X. Ren and K. Otsuka, Mater. Sci. Eng. A, 622(2006), 438.
[22] J.I. Kim, Y. Liu and S. Miyazaki, philos. Mag. A, 20(2004), 2083.
[23] G.R. Purdy, J.G. Parr, Trans. Metal. Soc. AIME, 221(1961), 636.
[24] F.E. Wang, W.J. Buheler, S.J. Pickart, J. Appl. Phys., 36(1965), 3232.
[25] J. E. Hanlon, S.R. Butler and R.J. Wasilewski, Trans. Metal. Soc. AIME, 239(1967), 1323.
[26] W. Tang, B. Sundmann, R. Sandstrom and C. Quiu, Acta Mater. , 47(1999), 3457.
[27] J. Khalil-Allafi, A. Dlouhy and G. Eggeler, Acta Mater. , 50(2002), 4255.
[28] J. Frenzel, E.P. George, A. Dlouhy, Ch. Somsen, M.F. X. Wagner and G. Eggeler , Acta Mater. , 58(2010), 3444.
[29] B. Karbakhsh Ravari, N. Kizakibaru and M. Nishida, J. Alloys Compd., 577S (2013), S268.
[30] B. Karbakhsh Ravari, M. Nishida, Philos. Mag., 193(2013), 2279.
[31] S. Cao, M. Nishida and D. Schryvers, Acta Mater. , 59(2011), 1780.
[32] M. Itakura, N. Kuwano, K. Sato and S. Tachibana, J. Electron Microsc., 59 Supple 1(2010), 165.